RSC Advances

PAPER

View Article Online
View Journal | View Issue

Cite this: *RSC Adv.*, 2025, **15**, 36116

Simulation study on selective recovery of Cu from Cu–Co–Ni composite system by Fe-struvite composite

Xingxing Wang *[a] and Xun Li[b]

The selective recycling of heavy metals is of great economic and environmental importance to human production and life. In this paper, the Fe-struvite composite (FSC) was synthesized by chemical principles and crystal growth theory, and further experimental methods such as model fitting, batch passivation experiment, mineral characterization, and chemical determination were used to explore the fixation properties and mechanisms of FSC on Cu–Co–Ni. The results demonstrate that FSC is an irregular composite of nano zero-valent iron loaded struvite. The passivation of Cu by FSC is multilayer (Q_{max} = 166.67 mg g^{-1}), whereas the adsorption of Co/Ni is monolayer. The passivations of Cu, Co and Ni by FSC are all physicochemical adsorption processes dominated by chemisorption. Nano-zero-valent iron undergoes the redox reaction with Cu and is accompanied by the formation of Fe^{2+}. Furthermore, NO_3^- weakly reduces the selective immobilization of Cu by FSC through reductive competition with Cu. Studies have shown that the passivation of Cu/Co/Ni by FSC is related to phase change, chelation/complexation, redox action and ion exchange, whereas the selective immobilization of Cu is related to differences in the physical properties of Cu/Co/Ni-PO_4 and Cu concentration. This study provides theoretical basis for the selective recovery of Cu using FSC.

Received 25th May 2025
Accepted 14th September 2025

DOI: 10.1039/d5ra03673a

rsc.li/rsc-advances

1. Introduction

Copper has superior electrical and thermal conductivity, ductility, corrosion resistance, and unique antimicrobial properties, which have made it an indispensable basic material in modern industrial and agricultural fields such as energy, healthcare, construction, and transport.[1–5] As the trend towards renewable energy, electrification and sustainability accelerates, the demand for copper increases significantly.[5] Due to the scarcity of copper resources, our country needs to import a large amount of copper mineral resources from abroad every year.[2] However, Cu mineral resources are concentrated in countries such as Congo, Canada and Russia, making the supply chain vulnerable to international politics and environmental protection.[6,7] Therefore, the recycling of copper resources is one of the important ways to cope with the shortage of copper resources in China at present. Studies have shown that Co/Ni often forms composite deposits with Cu and other elements, leading to serious Co–Ni–Cu composite environmental heavy metal pollution during mineral extraction, which in turn poses a great threat to human health and ecological security.[8,9] Moreover, the production and processing of Cu generates a large amount of industrial wastewater (including Co, Ni, Cu, *etc*), and wastewater discharge will cause huge economic losses.[10–15] Therefore, the separation, extraction and recycling of copper resources is an important research topic to address the needs of social development and environmental pollution control.

Selective enrichment separation is one of the key technologies for the recovery and reuse of copper resources, and limited research has been conducted in this area. Yang *et al.* (2024) prepared functionalized Ui-66 composites using thiophene schiff bases, which achieved selective adsorption of copper ions by forming a special ligand structure with them.[16] The ammonium pyrrolidine dithiocarbamate-modified biochar can achieve highly selective adsorption of copper ions through a unique chelating mechanism.[17] Ji *et al.* (2021) have prepared unique gel particles using cross-linking and freeze-drying methods, which can achieve selective adsorption of copper ions through a slit-like structure.[18] Jia *et al.* (2025) prepared surface ion-imprinted sodium alginate silica composites that not only selectively adsorb copper but also catalyze the formation of methanol from CO_2.[19] Although some academic achievements have been made in the separation and extraction of copper ions, the high cost of material preparation, complexity of the process and low selective separation capacity mean the existing technology still needs further development.[20–22]

Magnetic separation of heavy metals is one of the effective ways to reduce the cost of heavy metal wastewater treatment.[23]

[a]*College of Life Sciences, Anqing Normal University, Anqing 246133, China. E-mail: 1074136908@qq.com*

[b]*Nanjing Vocational Health College, Jiangsu Union Technical Institute, Nanjing 210038, China*

Huang *et al.* (2020) prepared sulfhydryl-functionalized magnetic covalent organic frameworks using Fe_3O_4, which can efficiently magnetically separate Hg^{2+} from wastewater.[24] *Shewanella oneidenis* enhances Cr(VI) passivation and magnetic separation of secondary products by mediating the synthesis of zero-valent iron nanoparticles.[25] Although both Fe_3O_4 and nano zero-valent iron are common magnetic source materials, nano zero-valent iron has been widely used in environmental pollution treatment of water, soil and groundwater due to its large surface area, powerful oxidation properties and high surface activity.[26–31] Therefore, the multifunctional composites formed by using zero-valent iron nanoparticles as a source of magnetism have a promising use in the efficient and selective recycling of heavy metal.[32,33]

Struvite is a sub-stable phosphate mineral, which has an important impact on the transport and transformation of environmental heavy metals.[34–38] Our previous studies found that struvite exhibits highly selective adsorption properties for copper under certain specific circumstances, but the immobilization characteristics and mechanism are not clear.

Therefore, this article adopts chemical methods to synthesize Fe-struvite composite (FSC), and combines various experimental methods such as chemical analysis, batch adsorption, and mineral characterization to explore its competitive and selective passivation characteristics and mechanisms for Cu–Co–Ni. This study provides basic information on the separation and extraction of Cu by FSC.

2. Materials and methods

2.1. Material synthesis

The 200 mL of 80% aqueous ethanol solution was prepared using anhydrous ethanol and ddH_2O in a glass beaker, and 40 mL of the prepared ethanol solution was pipetted into a 50 mL EP tube using a pipette gun. The 1.0788 g KBH_4 was weighed on an analytical electronic balance and placed in a 50 mL EP tube containing 40 mL of ethanol solution and allowed to dissolve as much as possible. An analytical electronic balance was used to weigh 1.6218 g $FeCl_3 \cdot 6H_2O$, which was poured into a 200 mL glass beaker containing the remaining ethanol solution. The beaker was placed on a magnetic rotator for stirring (400 rpm, 25 °C) and the KBH_4 solution was aspirated with a pipette gun and slowly added to the ferric chloride solution, which was spun for 10 min after the operation. The precipitates were then washed 3 times with ddH_2O and the supernatant was poured out after fixing the precipitates with a magnet.

The 100 mL ddH_2O was added to the above beaker containing the precipitate with magnetic stirring (400 rpm, 25 °C). An analytical electronic balance was used to weigh 2.3128 g $Na_2HPO_4 \cdot 12H_2O$ and 1.5274 g NH_4Cl and add them to the above beaker. Then, 0.7836 g $MgCl_2 \cdot 6H_2O$ was added to the aforementioned beaker, and the mixture was continuously stirred for 10 min. The precipitated compounds were rinsed several times with ddH_2O at the end of mixing and transferred to new 50 mL EP

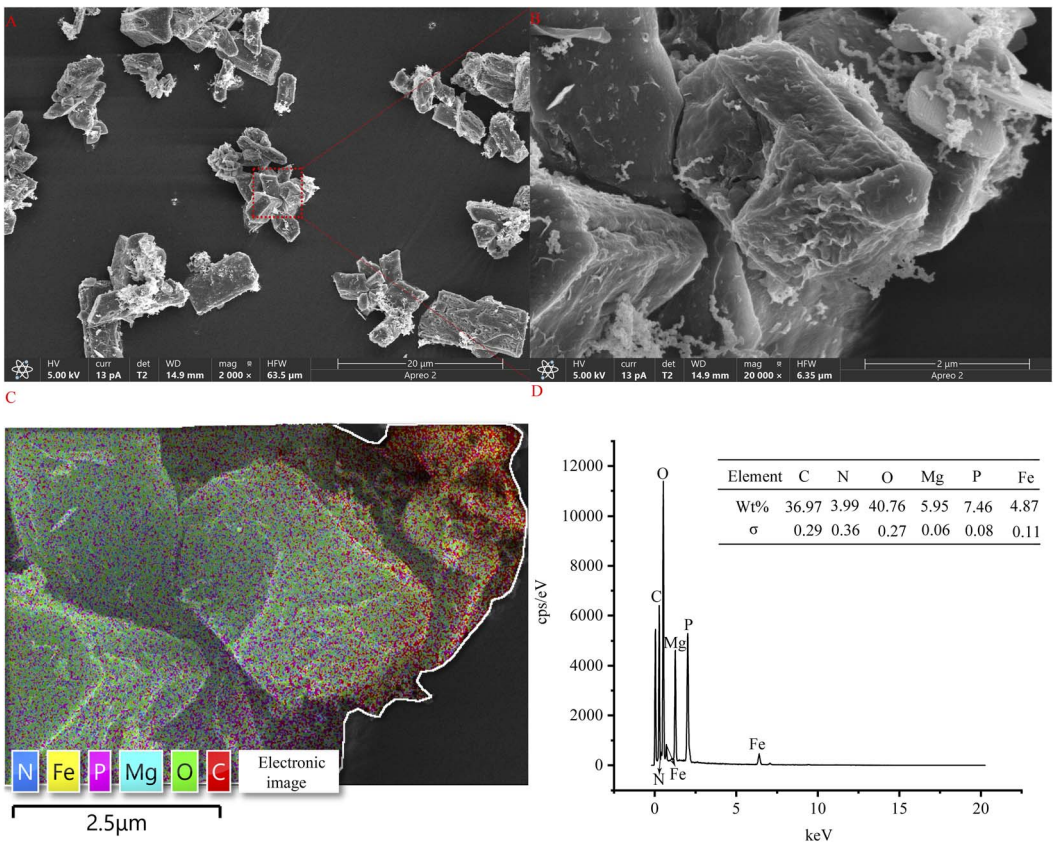

Fig. 1 The characterization of the morphology and elemental composition of FSC (A and B) SEM; (C) Elemental electron image; (D) EDS.

tubes. Finally, this EP tube was lyophilized and the material was used as an adsorbent for subsequent experiments.

2.2. Adsorption isotherm

$CuCl_2 \cdot 2H_2O$, $CoCl_2 \cdot 6H_2O$, $NiCl_2 \cdot 6H_2O$ and ddH_2O were used to prepare heavy metal solutions of different concentrations (Cu: 4.88–397.96 mg L^{-1}, Co: 4.95–406.94 mg L^{-1}, Ni: 4.45–378.36 mg L^{-1}). Subsequently, ddH_2O and the above chemicals were used to formulate aqueous solutions of different binary systems of heavy metals (Cu: 4.69–381.86 mg L^{-1} + Ni: 4.78–394.12 mg L^{-1}, Cu: 4.71–387.74 mg L^{-1} + Co: 4.83–409.49 mg L^{-1}, Co: 4.72–414.63 mg L^{-1} + Ni: 4.73–387.42 mg L^{-1}), and binary heavy metal concentrations were combined in descending order of similar concentrations. Finally, different concentrations of ternary heavy metal solutions (Cu: 4.63–382.20 mg L^{-1} + Co: 4.80–395.3 mg L^{-1} + Ni: 4.86–415.66 mg L^{-1}) were prepared using ddH_2O and chemical reagents, and the ternary heavy metal concentrations were compounded according to the similar concentrations in order from the lowest to the highest.

The 20 mL solutions of the various heavy metals compounds at different concentrations described above were pipetted into several 50 mL EP tubes using a pipette gun, with three separate replicates at each concentration of each heavy metal compound. Several parts (0.01 g/serving) of the adsorbent were weighed using an analytical electronic balance. The experimental system was incubated for 24 h (25 °C, 100 rpm) after adsorbents were added to each of tubes. At the end of the adsorption, the samples were centrifuged (9000 rpm, 25 °C, 5 min) and the supernatant was collected. The concentrations of Cu, Co, Ni, Mg and Fe in the supernatant were determined using a flame atomic spectrophotometer (AAS, AA-6300C, Shimadzu) and the NH_4^+ concentration was determined using a spectrophotometer (BD15/T 1458-2018). The eqn (1) was used to calculate the passivation capacity of heavy metals by adsorbent.[39]

Furthermore, Langmuir and Freundlich equations were further used to fit the above experimental data.[40]

$$Q_e = (C_o - C_e)/M \times V \quad (1)$$

Q_e: immobilization capacity at passivation equilibrium, mg g^{-1}; C_o: heavy metal initial concentration, mg L^{-1}; C_e: pollutant concentration at passivation equilibrium, mg L^{-1}; M: material utilization amount, g; V: experimental volume, mL.

2.3. Adsorption kinetic

$CuCl_2 \cdot 2H_2O$, $CoCl_2 \cdot 6H_2O$, $NiCl_2 \cdot 6H_2O$ and ddH_2O were used to prepare heavy metal solutions at specific concentrations for different composite systems (374.21 mg L^{-1} Cu, 423.13 mg L^{-1} Co, 347.95 mg L^{-1} Ni, 385.78 mg L^{-1} Cu + 405.53 mg L^{-1} Co, 384.36 mg L^{-1} Cu + 372.58 mg L^{-1} Ni, 405.20 mg L^{-1} Co +

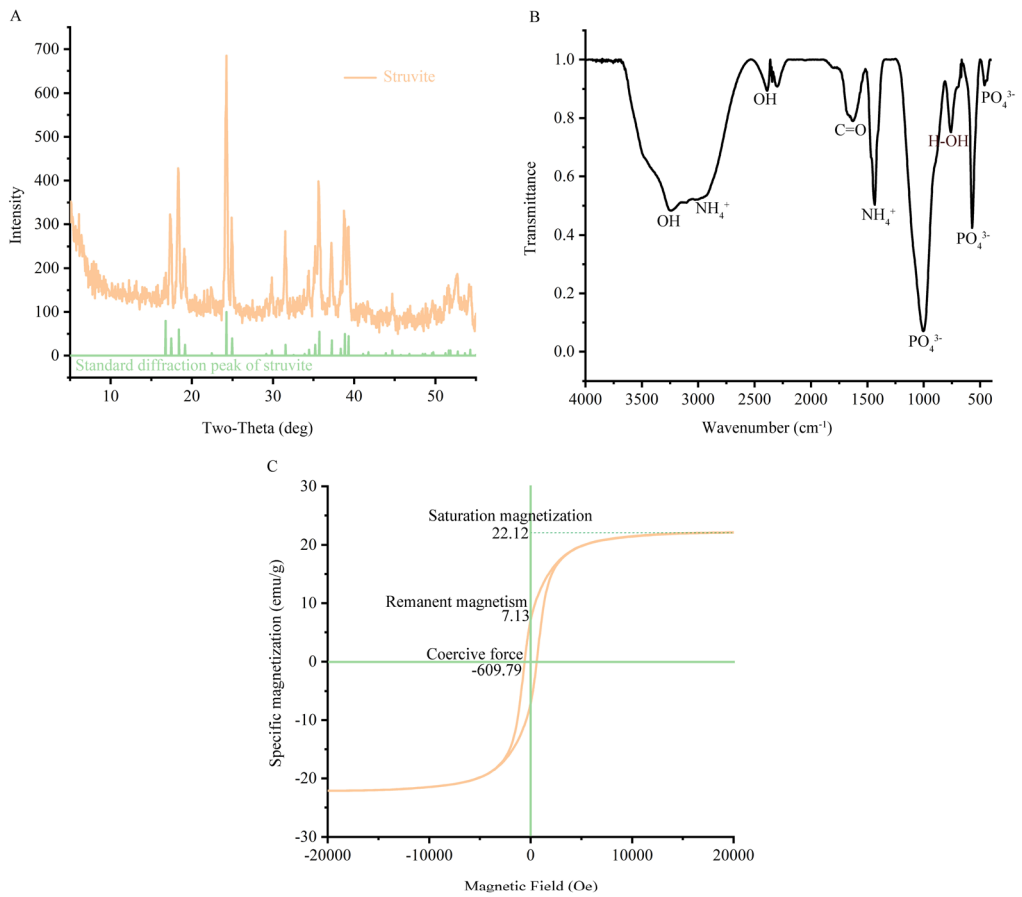

Fig. 2 The physicochemical properties of FSC (A) XRD; (B) FTIR; (C) Hysteresis curve.

379.83 mg L^{-1} Ni, 379.06 mg L^{-1} Cu + 381.06 mg L^{-1} Co + 377.78 mg L^{-1} Ni). Appropriate portions of 20 mL adsorption liquid of different composite systems were pipetted into 50 mL EP tubes using a pipette gun (three replicates per treatment). Multiple adsorbents (0.01 g/serving) were weighed using an analytical electronic balance and the adsorbent was added to each of the above 50 mL tubes. The experimental system was then incubated in a shaker with shaking (25 °C, 100 rpm). Three centrifuge tubes were centrifuged (25 °C, 9000 rpm, 5 min) at specific point in time (time points: 5–720 min). The concentration of Cu/Co/Ni in the supernatant was detected by AAS. The eqn (1) was used to calculate the passivation ability of Cu/Co/Ni. Based on the experimental results, the pseudo-first-order dynamic equation and pseudo-second-order dynamic equation were used to fit the experimental data.[41]

2.4. Material characterization

The morphology and elemental composition of the materials before and after adsorption were characterized using scanning electron microscopy microscopy and energy spectroscopy (SEM-EDS, Apreo 2S + – Oxford ultim max 65, Thermo Fisher Scientific). The mineral crystal structure and organic functional group before and after adsorption were studied using the X-ray diffractometer (XRD, BTX-526, Olympus, USA) and the infrared spectrometer (FTIR, Nexus 670, Thermo Nicolet). The magnetic strength and associated elemental valence states of the samples before and after adsorption were characterized using the

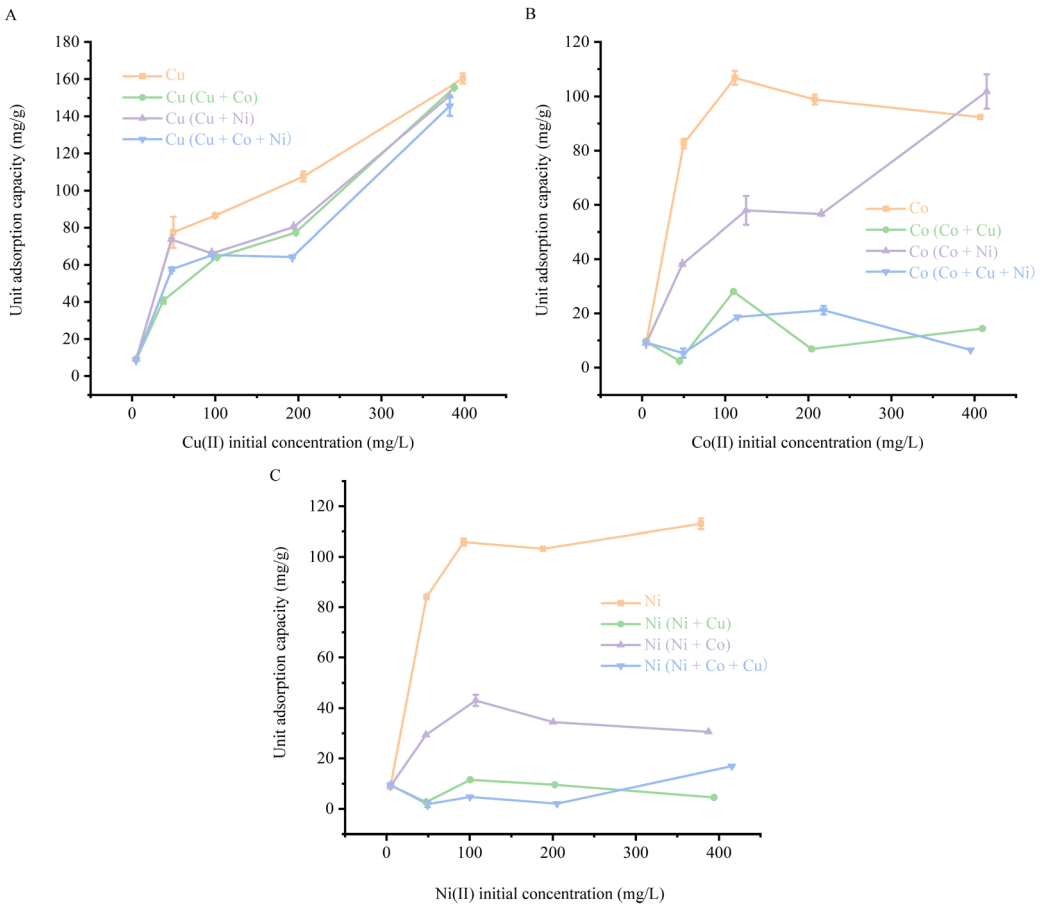

Fig. 3 The passivation of Cu/Co/Ni by FSC in different passivation systems (A) Cu; (B) Co; (C) Ni.

Table 1 The adsorption isothermal parameters

		Langmuir			Freundlich		
Treatment	Heavy metal	Q_{max} (mg g^{-1})	K_L (L mg^{-1})	R^2	ln K_F (L mg^{-1})	$1/n$	R^2
Unitary system	Cu	166.67	0.03	0.9283	2.82	0.39	0.9938
	Co	121.95	0.22	0.9995	3.62	0.30	0.6922
	Ni	113.64	0.55	1.0000	3.38	0.30	0.8886
Ternary system	Cu	135.14	0.02	0.6846	2.82	0.34	0.9363
	Co	28.33	0.01	0.4990	2.24	0.09	0.1729
	Ni	3.67	0.08	0.9292	1.84	0.16	0.6258

vibrating sample magnetometer (VSM, LakeShore 7404, USA) and the X-ray photoelectron spectrometer (XPS, Thermo Fisher ESCALAB 250Xi, USA).

Table 2 The competition constants and interaction effects of Cu/Co/Ni in the ternary adsorption systems

Pollutants	Competitive constants		Interactive effect
	$Q_{mixture}/Q_{single}$	$\Delta Y\%$	
Cu	0.81	18.92	Poor antagonistic
Co	0.23	76.77	Strong antagonistic
Ni	0.03	96.77	Strong antagonistic

3. Results and discussion

3.1. Material characterization

The study of physicochemical properties is an important part of adsorbent, and the study results of material properties are shown in Fig. 1 and 2. During the course of the experimental manipulation, it is observed that the mineral changes from black to light grey, presumably forming a core–shell structure (Fe is inside and struvite is outside). The adsorption materials synthesized in this work exhibit an irregular morphology (Fig. 1A). The enlarged image shows that the surface of the mineral is rough and contains nanoscale bead-like structures in certain areas (Fig. 1B), which are thought to be nano zero-valent

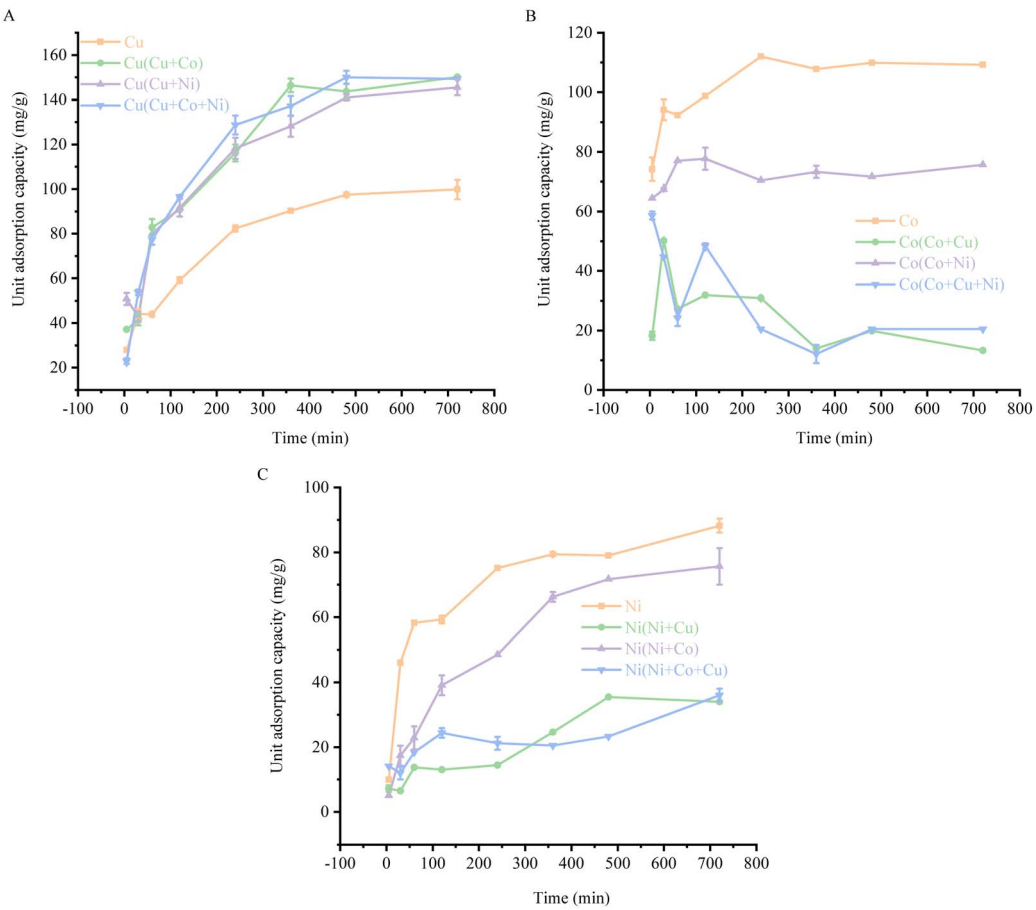

Fig. 4 The effect of immobilization time on the adsorption of Cu/Co/Ni by FSC in different passivation systems (A) Cu; (B) Co; (C) Ni.

Table 3 The adsorption kinetic parameters

Treatment	Heavy metal	Pseudo-first-order kinetic			Pseudo-second-order kinetic		
		Q_e (mg g^{-1})	K_1 (min^{-1})	R^2	Q_e (mg g^{-1})	K_2 (g mg^{-1} min^{-1})	R^2
Unitary system	Cu	91.74	39.75	0.7922	111.11	0.00	0.9944
	Co	105.26	2.17	0.8616	111.11	0.00	0.9995
	Ni	92.59	41.09	0.9962	85.47	0.00	0.9973
Ternary system	Cu	91.74	39.75	0.7922	111.11	0.00	0.9944
	Co	22.68	3.44	0.2278	18.66	0.00	0.8829
	Ni	19.65	2.36	0.3041	22.94	0.00	0.9896

iron.[42,43] The EDS results show that the mineral consists of Mg, O, P, N, Fe, and C (Fig. 1C and D). The Mg, O, P, and N are the constituents of struvite. The element Fe is derived from zero-valent iron nanoparticles or synthetic raw materials, and C is supposed to be derived from carbon-based compounds such as ethanol during the synthesis of zero-valent iron.

The XRD results show that the synthesized material mainly consists of crystalline struvite, but no peaks of nano zero-valent iron were compared (Fig. 2A), suggesting that the nano zero-valent iron may be an amorphous mineral.[44] The FTIR results reveal that organic functional groups (–OH/C=O/COO^-) is observed on the surface of material (Fig. 2B), indicating that the material is an organic–inorganic composite.[45–47] Furthermore, the magnetic data show an overall elongated hysteresis curve (Ms = 22.12 emu g^{-1}, Mr = 7.13 emu g^{-1}, Hc = 609.79 O_e), indicating that the adsorption material is hard magnetic materials (Fig. 2C).[48] Based on the above results, it is clear that the material synthesized in this paper can be termed as Fe-struvite composite (FSC).

Table 4 The distribution and selectivity coefficient of Cu/Co/Ni in ternary system[a]

	K_d			k	
Time (min)	Cu	Co	Ni	Cu/Co	Cu/Ni
5	0.07	0.15	0.04	0.47	1.75
30	0.15	0.12	0.04	1.25	3.75
60	0.23	0.06	0.08	3.83	2.88
120	0.3	0.12	0.06	2.50	5.00
240	0.41	0.08	0.05	5.13	8.20
360	0.45	0.03	0.07	15.00	6.43
480	0.49	0.1	0.07	4.90	7.00
720	0.52	0.07	0.09	7.43	5.78

[a] Distribution coefficient $K_d = Q_t/C_t$, selectivity coefficient $k = K_d(Cu)/K_d(x)$, x = Co/Ni.

3.2. Adsorption isotherm

The adsorption isothermal parameters can well reveal the arrangement of heavy metals on the FSC, and the results of adsorption isothermal experiments of Cu/Co/Ni by FSC are

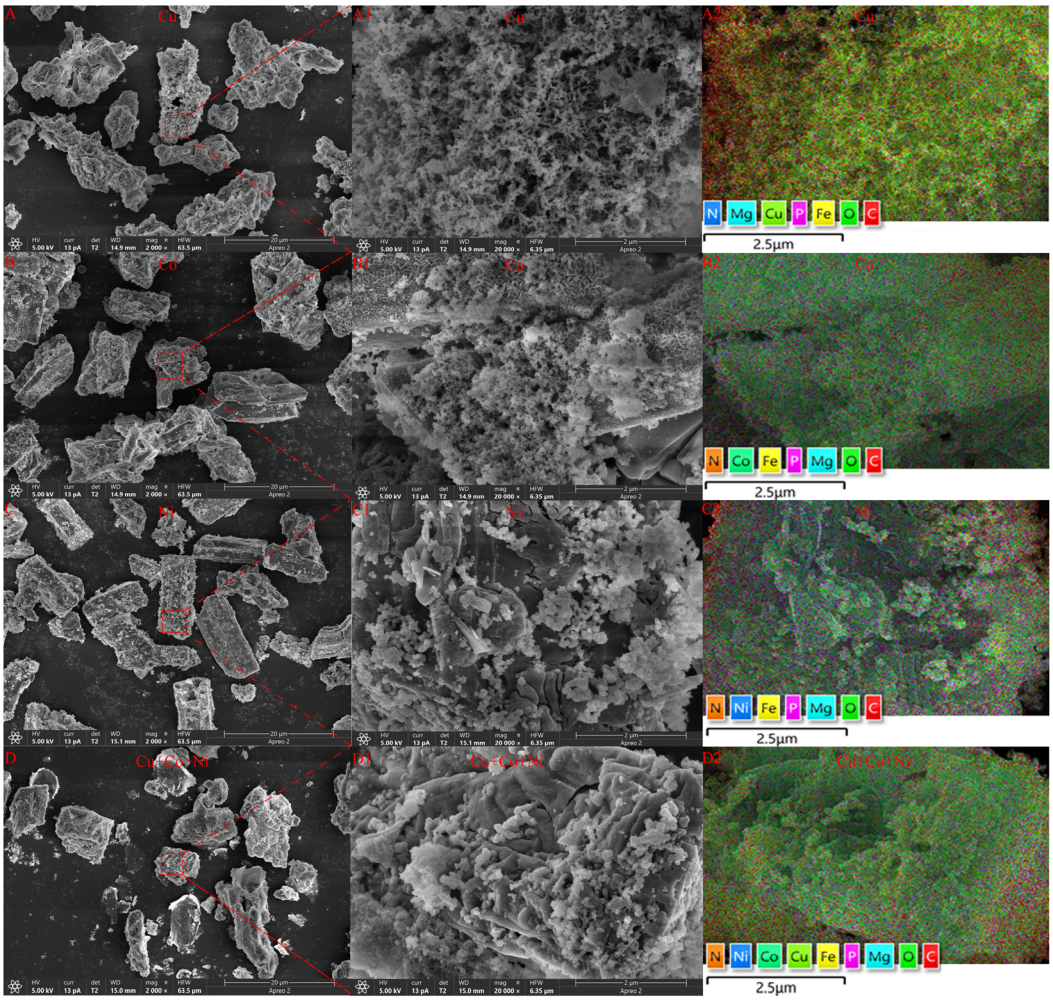

Fig. 5 The morphological and electronic images of precipitates after adsorption of Cu/Co/Ni by FSC (A, A1, B, B1, C, C1, D, and D1) SEM; (A2–D2) Elemental electron images.

shown in Fig. 3. The overall trend of Cu by FSC in different adsorption systems shows an increase with the initial Cu concentration (Fig. 3A). The presence of Co/Ni reduces the adsorption capacity of FSC for Cu, but to a lesser extent, which is attributed to the competitive adsorption between heavy metals (Fig. 3A). The adsorption of Co/Ni by FSC shows an overall trend of increasing and then levelling off, but the presence of other ions significantly reduces the adsorption of Co/Ni by FSC (Fig. 3B and C). The results of Fig. 3B and C show that the adsorption of Co/Ni is susceptible to competition from Cu, further revealing that the lower affinity of FSC for Co/Ni.[49] Additionally, the experimental data is further fitted using adsorption isothermal models (Table 1).

The passivation of Cu by FSC is better fitted by the Freundlich equation ($R^2 = 0.9938/0.9363$) (Table 1), indicating that the passivation of Cu by FSC is a multilayer adsorption.[50] The immobilization of Co/Ni by FSC is better fitted by Langmuir equation ($R^2 = 0.9995/0.4990$ and 1/0.9292), revealing that the adsorption of Co/Ni by FSC is monolayer adsorption.[51] Differences in the number of adsorbed layers may be related to the differences in hydration capacity of Cu/Ni/Co and their ability to bind to NH_4^+. Furthermore, K_L and $1/n$ are between 0 and 1, demonstrating that the adsorption of Cu/Co/Ni by FSC is prone to occur.[52] Further analysis shows that a strong competitive adsorption relationship is observed between Cu and Co/Ni (Table 2), which will provide useful information for the selective separation of Cu using FSC.

3.3. Adsorption kinetic

The type of interaction force between the adsorbent and the adsorbate is one of the important research contents in adsorption experiments, the adsorption kinetics of Cu/Co/Ni by FSC are shown in Fig. 4 and Table 3. The passivation of Cu by FSC shows a first gradually increase and then tends to parallel (Fig. 4A), which may be related to the time and manner of formation of copper-containing phosphate compounds. The adsorption of Co/Ni by FSC is similar to the adsorption of Cu by FSC, but the presence of other ions inhibits the adsorption of Co/Ni by FSC (Fig. 4B and C), indicating that FSC has a high affinity for Cu. Furthermore, the kinetic model fitting parameters are presented in Table 3.

Table 3 shows that the passivation of Cu, Co and Ni by FSC are all well fitted by pseudo-second-order kinetic ($R^2 = 0.9944/0.9944$, 0.9995/0.8829 and 0.9973/0.9896), displaying that the adsorption of Cu/Co/Ni by FSC is a physicochemical adsorption dominated by chemisorption.[53] Moreover, the results of the

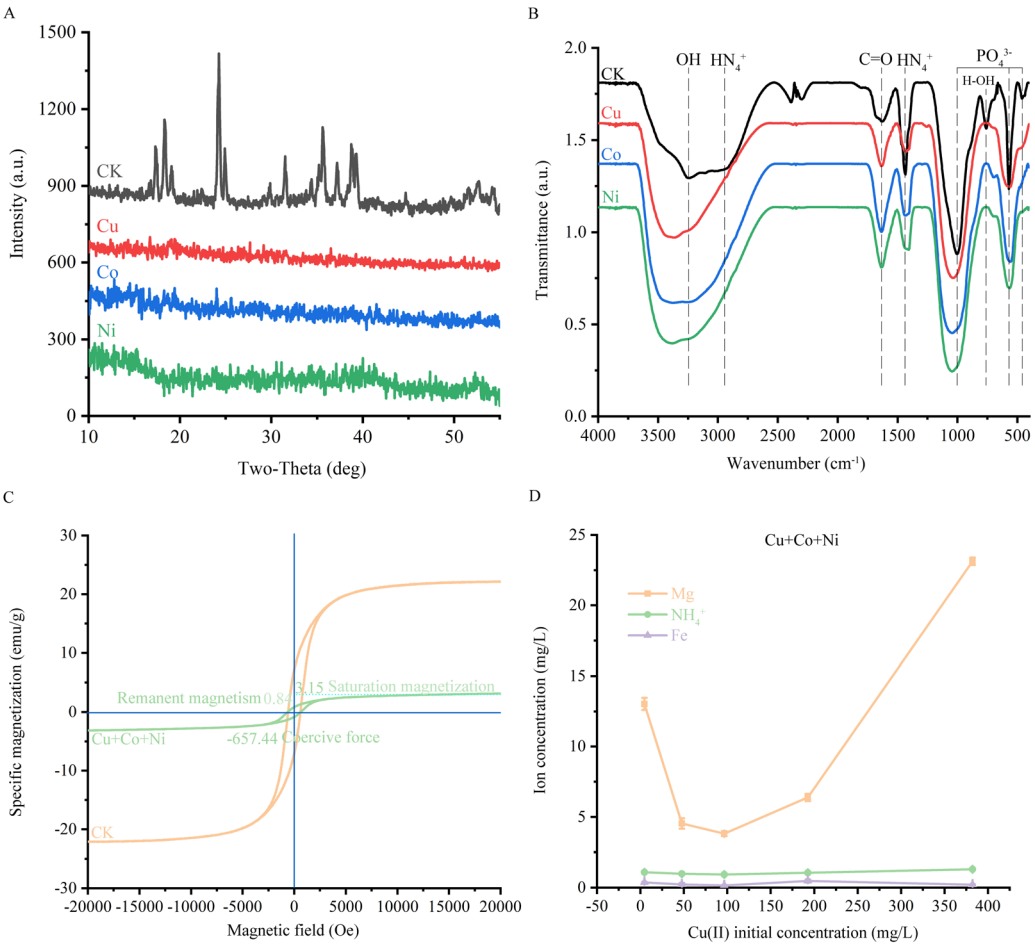

Fig. 6 The mechanistic analysis of Cu/Co/Ni passivation by FSC (A) XRD; (B) FTIR; (C) Hysteresis curve; (D) ion release capacity.

adsorption kinetic show that FSC has a selective sequestration capacity for Cu in the ternary composite system (Fig. 4, S1 and Table 3), which is related to the difference in the K_{sp} of Cu/Co/Ni-PO_4 and Cu concentration (Tables S1 and 2). To further quantify the selective fixation ability of FSC on Cu, the results of the selectivity coefficient and distribution coefficient are shown in Table 4. Table 4 shows that the k value has an increasing trend with the increasing of passivation time, indicating that FSC can efficiently and selectively enrich and separate Cu from the composite heavy metal solution. Furthermore, the FSC also has magnetic separation properties (Fig. 2C), which may provide a viable option for the separation and extraction of Cu and the remediation of Cu contamination in field environments.

4. Mechanism analysis

Revealing the immobilization mechanism of FSC on heavy metals helps to deepen the understanding of the interaction mechanism between FSC and Cu/Co/Ni, and the relevant results are shown in Fig. 5 and 6. The morphology of FSC adsorbed heavy metals changes significantly, with more secondary mineral particles appearing on the mineral surface (Fig. 5 A, A1, B, B1, C, C1, D and D1), and a large amount of Cu/Co/Ni is detected on the mineral surface (Fig. S2 and A2–D2). Additionally, the presence of Cu strongly reduces the content of Co/Ni (Fig. 5 and S2), which also indicates a strong competitive effect of Cu on Co/Ni.

After passivation of Cu/Co/Ni by FSC, the mineral crystal structure collapses and no new secondary crystalline is detected (Fig. 6A), which may be related to the fickleness of the struvite crystal and its high affinity for Cu/Co/Ni. The vibrational peaks of the NH_4^+ group are weakened or disappeared and the vibrational peaks of the PO_3^- group are weakened or red-shifted after the adsorption of Cu/Co/Ni by FSC (Fig. 6B), which is related to the combination of PO_3^- with Cu/Co/Ni and the release of NH_4^+.[54] In addition, the –OH/C=O is red-shifted (Fig. 6B), which is related to the combination of –OH/C=O and Cu/Co/Ni.[22] The magnetization strength of the secondary mineral reduces significantly (Ms = 3.15 emu g^{-1}, Mr = 0.84 emu g^{-1}, and Hc = 657.44 Oe) (Fig. 6C), which may be related to the decrease in zero-valent iron content. However, it is still possible to separate secondary mineral using magnetism in the presence of the externally enhanced magnetic field. Further studies show

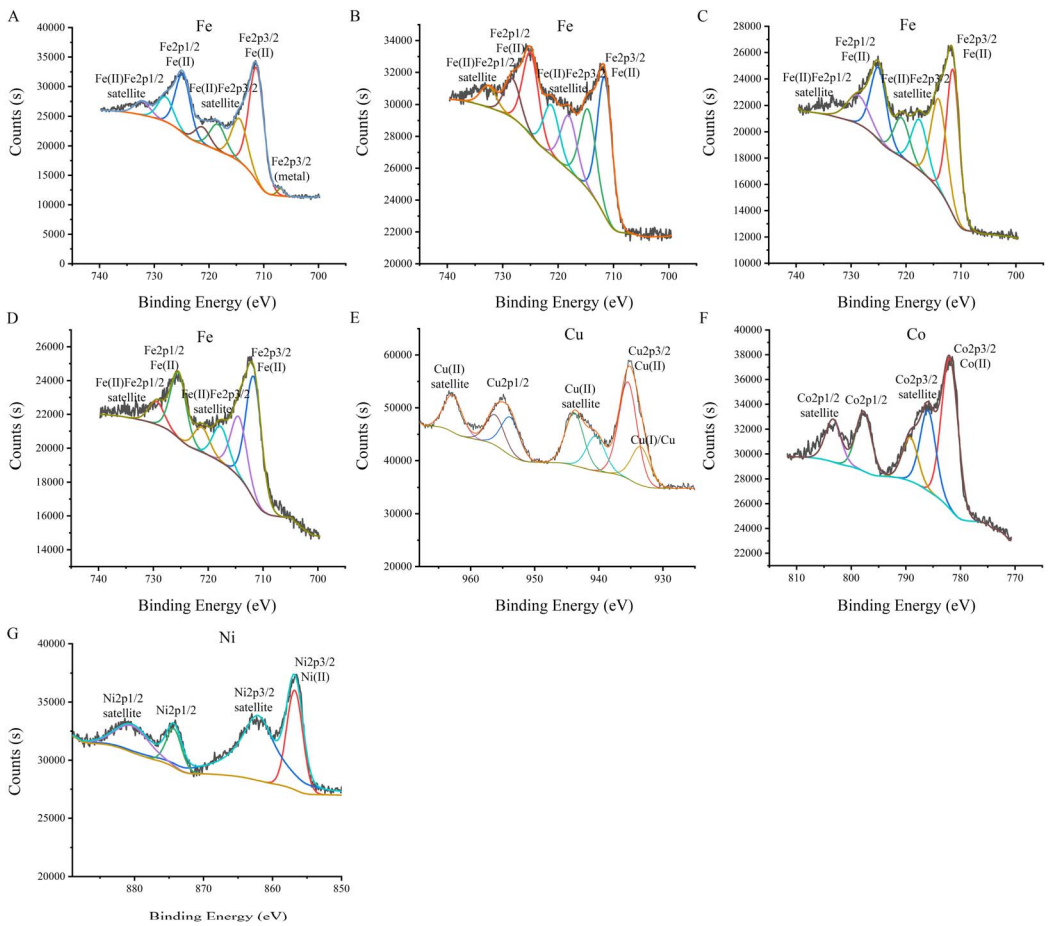

Fig. 7 The XPS of FSC after adsorption of heavy metals (A) Fe2p of FSC; (B) Fe2p of FSC after adsorption of Cu(II); (C) Fe2p of FSC after adsorption of Co(II); (D) Fe2p of FSC after adsorption of Ni(II); (E) Cu2p of FSC after adsorption of Cu(II); (F) Co2p of FSC after adsorption of Co(II); (G) Ni2p after FSC adsorption of Ni(II).

that the passivation of Cu/Co/Ni by FSC results in the release of NH_4^+, Mg^{2+} and Fe^{2+} (Fig. 6D), suggesting that the adsorption of Cu/Co/Ni by FSC involves ion exchange. Zero-valent iron nanoparticles are highly oxidation, which may lead to changes in the valence state of Cu/Co/Ni, the results are shown in Fig. 7. The XPS results show the presence of Fe^{2+} and zero-valent iron in FSC (Fig. 7A), indicating that the FSC contains nano zero-valent iron. After adsorption of Cu/Co/Ni by FSC, the zero-valent iron disappear and only Fe^{2+} is detected (Fig. 7A–D), which indicates that the nano-zero-valent iron might undergo a redox reaction with Cu/Co/Ni. Further study shows that only a change in the valence state of Cu was detected (Fig. 7E–G), which may be related to factors such as differences in standard reduction potentials, the size of the kinetic barrier to the reaction and the chemical condition of the surface.

Additionally, reducing substances such as NO_3^- are commonly found in the environment and may affect the selective passivation of Cu by FSC. Therefore, the effect of reducing substances represented by NO_3^- on the selective passivation of Cu by FSC is investigated. The results shows that the presence of NO_3^- slightly reduces the selective adsorption capacity of FSC for Cu (Fig. S3). Fig. S4A shows that the presence of Co, Ni and NO_3^- leads to an increase in the slope of the curve at 933 eV together with an increase in the number of burrs, suggesting a weakening of the reduction of Cu. Fig. S4B shows that the presence of Co/Ni and NO_3^- significantly reduces the photoelectron intensity of Cu, which suggests that the presence of Co/Ni and NO_3^- inhibits the reduction action of Cu.

5. Conclusion

FSC is an irregularly shaped organic–inorganic mineral composite of nano zero-valent iron loaded struvite. The adsorption of Cu by FSC is multilayer, whereas the adsorption of Co/Ni is monolayer. The adsorption of Cu, Co and Ni by FSC are all physicochemical adsorption processes dominated by chemisorption. Phase change occurs in all of the Cu/Co/Ni adsorption by FSC, and both Mg^{2+} and NH_4^+ are ion-exchanged with Cu/Co/Ni. Zero-valent iron nanoparticles undergo redox reactions with Cu accompanied by the formation of Fe^{2+}, and NO_3^- weakly reduces the selective sequestration of Cu by FSC through competition with Cu for reduction action. Furthermore, FSC selectively passivates Cu in a variety of complex heavy metal ion systems. Studies have shown that the passivation of Cu/Co/Ni by FSC is related to phase change, ion exchange, redox and complexation/chelation, whereas the selective enrichment and separation properties of Cu is related to physical properties of Cu/Co/Ni-PO_4 and Cu concentration. This study provides theoretical basis for the selective recycling of Cu using FSC.

Author contributions

Xingxing Wang: conceptualization, investigation, experiments, data curation, data analysis & interpretation, writing – original draft, writing – review & editing; Xun Li: writing – original draft, writing – review & editing.

Conflicts of interest

The authors declare that they have no known competing financial interests or personal relationships that could have appeared to influence the work reported in this paper.

Data availability

Data will be made available on request.

Supplementary information is available. See DOI: **https://doi.org/10.1039/d5ra03673a**.

Acknowledgements

This study was supported by the Doctoral Scientific Startup Fund from Anqing Normal University (Grant No. 251052).

References

1 C. H. Lin, New Cu(TiBNx) copper alloy films for industrial applications, *Jpn. J. Appl. Phys.*, 2016, **55**, 06JD02.
2 S. H. Sun, Z. H. Meng, M. L. Li, X. H. Yang and X. X. Wang, Global supply sustainability assessment of critical metals for clean energy technology, *Resour. Policy*, 2023, **85**, 103994.
3 B. K. Sovacool, S. H. Ali, M. Bazilian, B. Radley, B. Nemery, J. Okatz and D. Mulvaney, Sustainable minerals and metals for a low-carbon future, *Science*, 2020, **367**, 30–33.
4 S. H. Ali, D. Giurco, N. Arndt, E. Nickless, G. Brown, A. Demetriades, R. Durrheim, M. A. Enriquez, J. Kinnaird, A. Littleboy, L. D. Meinert, R. Oberhansli, J. Salem, R. Schodde, G. Schneider, O. Vidal and N. Yakovleva, Mineral supply for sustainable development requires resource governance, *Nature*, 2017, **543**, 367–372.
5 M. P. Van Hoecke and M. J. F. Leroy, Metals: supply shortage of strategical raw materials, *Actual. Chim.*, 2011, **358**, 24–29.
6 J. L. H. Cailteux, A. B. Kampunzu, C. Lerouge, A. K. Kaputo and J. P. Milesi, Genesis of sediment-hosted stratiform copper–cobalt deposits, central African Copperbelt, *J. Afr. Earth Sci.*, 2005, **42**, 134–158.
7 K. B. Shedd, E. A. Mccullough and D. I. Bleiwas, Global trends affecting the supply security of cobalt, *Min. Eng.*, 2017, **69**, 37–42.
8 B. X. Sun, S. Y. Jiang, M. M. Cui, Q. H. Yuan and L. Z. Yan, Progress in mineralization and prospecting technology of cobalt and nickel: preface, *Acta Petrol. Sin.*, 2023, **39**, 963–967.
9 A. K. Saim and F. K. Darteh, A comprehensive review on cobalt bioleaching from primary and tailings sources, *Min. Proc. Ext. Met. Rev.*, 2024, **45**, 28.
10 Z. Liu, L. Wang, Y. Jiang, Y. Lv, C. Zhu, F. Liu and A. Li, Dialysis technology supporting the preparation of acid-resistant picolylamine-based hydrogel sphere for selectively recycling copper, nickel and cobalt from strongly acidic wastewaters, *Chem. Eng. J.*, 2022, **450**, 138329.
11 K. Khan, M. Younas, M. Yaseen, H. Sher, A. Maryam, S. M. Ibrahim, A. Adnan, A. Ali, M. Fawad, A. Z. Khan, N. Khan and I. A. Shah, Heavy metals pollution in riverine

sediments: distribution, source, and environmental implications, *Environ. Monit. Assess.*, 2025, **197**, 225.

12 H. Zhou, Y. Chen, Y. Liu, Q. Wang and Y. Liang, Farmers' adaptation to heavy metal pollution in farmland in mining areas: the effects of farmers' perceptions, knowledge and characteristics, *J. Clean. Prod.*, 2022, **365**, 132678.

13 G. Yu, L. Wu, Q. Su, X. Ji, J. Zhou, S. Wu, Y. Tang and H. Li, Neurotoxic effects of heavy metal pollutants in the environment: focusing on epigenetic mechanisms, *Environ. Pollut.*, 2024, **345**, 123563.

14 F. Yan, N. Li, J. Wang and H. Wu, Ecological footprint model of heavy metal pollution in water environment based on the potential ecological risk index, *J. Environ. Manag.*, 2023, **344**, 118708.

15 Y. G. Chen, X. L. He, J. H. Huang, R. Luo, H. Z. Ge, A. Wolowicz, M. Wawrzkiewicz, A. Gladysz-Plaska, B. Li, Q. X. Yu, D. Kolodynska, G. Y. Lv and S. H. Chen, Impacts of heavy metals and medicinal crops on ecological systems, environmental pollution, cultivation, and production processes in China, *Ecotoxicol. Environ. Saf.*, 2021, **219**, 112336.

16 Y. Yang, Y. Wang, Q. G. Gou, Y. Y. Zhang, Y. Q. Wu and Y. H. Luo, Synthesis of thiophene Schiff base functionalized UiO-66 for enhanced Cu(II) ion adsorption capacity and selectivity, *J. Solid State Chem.*, 2024, **332**, 124599.

17 T. M. A. Babeker, S. Lv, M. N. Khalil, Z. Hao and Q. Y. Chen, Biochar modified by ammonium pyrrolidine dithiocarbamate for high selective adsorption of copper in wastewater, *Sep. Purif. Technol.*, 2025, **352**, 129436.

18 C. Ji, S. Y. Yang, T. E, Y. Cheng, X. Hao and Y. Li, Three-dimensional network graphene oxide/sodium alginate aerogel beads with slit-shaped structure: synthesis, performance and selective adsorption mechanism for Cu(II), *J. Environ. Chem. Eng.*, 2021, **9**, 106819.

19 A. Jia, C. L. Chi, W. Dong, X. Y. Xu and H. L. Zhang, Hierarchical surface ion-imprinted sodium alginate/silica composite spheres for selective adsorption Cu(II) from wastewater and subsequently being transformed into an efficient photocatalyst for reducing CO_2 to methanol, *J. Environ. Chem. Eng.*, 2025, **13**, 115169.

20 W. H. Li, S. Y. Yang, Y. F. Wang, C. Peng, Y. Li and T. E, Selective adsorption of Cu(II) on amino-modified alginate-based aerogel: as a catalyst for the degradation of organic contaminant, *Int. J. Biol. Macromol.*, 2024, **278**, 134700.

21 Y. Y. Zhang, K. Yuan, L. Magagnin, X. S. Wu and Z. Y. Jiang, Selective adsorption of Pb(II) and Cu(II) on mercapto-functionalized aerogels: experiments, DFT studies and LCA analysis, *J. Clean. Prod.*, 2023, **393**, 136126.

22 L. Zhang, F. Yang, Y. Zhao, L. L. Zhong, R. H. Gao, X. M. Zhang, T. Wang and J. Q. Xue, Preparation of thiosemicarbazide-modified polyvinyl alcohol and its selective adsorption of Cu(II), *J. Colloid. Interf. Sci.*, 2021, **43**, 100377.

23 F. S. A. Khan, N. M. Mubarak, M. Khalid, R. Walvekar, E. C. Abdullah, S. A. Mazari, S. Nizamuddin and R. R. Karri, Magnetic nanoadsorbents' potential route for heavy metals removal - a review, *Environ. Sci. Pollut. Res.*, 2020, **27**, 24342–24356.

24 L. J. Huang, R. J. Shen, R. Q. Liu and Q. Shuai, Thiol-functionalized magnetic covalent organic frameworks by a cutting strategy for efficient removal of Hg^{2+} from water, *J. Hazard. Mater.*, 2020, **392**, 122320.

25 H. R. Tian, Q. Y. Wu, Q. J. Wu, C. Y. Sun, R. M. Zhang, J. Wei, H. Y. Xu, Z. M. Liu, C. Huang and P. Wang, Carbon nanotubes mediate electron transfer between *Shewanella oneidenis* MR-1 and nano zero-valent iron to enhance the elimination of Cr(VI) from aqueous media, *Sep. Purif. Technol.*, 2024, **341**, 126909.

26 W. Liang, G. Wang, C. Peng, J. Tan, J. Wan, P. Sun, Q. Li, X. Ji, Q. Zhang, Y. Wu and W. Zhang, Recent advances of carbon-based nano zero valent iron for heavy metals remediation in soil and water: a critical review, *J. Hazard. Mater.*, 2022, **426**, 127993.

27 A. Latif, D. Sheng, K. Sun, Y. Si, M. Azeem, A. Abbas and M. Bilal, Remediation of heavy metals polluted environment using Fe-based nanoparticles: mechanisms, influencing factors, and environmental implications, *Environ. Pollut.*, 2020, **264**, 114728.

28 M. M. Tarekegn, A. M. Hiruy and A. H. Dekebo, Nano zero valent iron (nZVI) particles for the removal of heavy metals Cd^{2+}, Cu^{2+} and Pb^{2+} from aqueous solutions, *RSC Adv.*, 2021, **11**, 18539–18551.

29 M. Xi, X. Zhang, G. Chen, L. Zhang, Z. Jiang and H. Zheng, Synergizing carbon sequestration mechanisms during the remediation of Cr(VI) by nano zero-valent iron loaded biochar (nZVI-BC), *J. Environ. Chem. Eng.*, 2024, **12**, 114781.

30 S. Krithika Shree, S. K. R. Namasivayam and A. Pandian, Sustainable developmental measures for the treatment of pharmaceutical industry effluent using nano zero valent iron technology (nZVI) – a review, *J. Water Process Eng.*, 2023, **56**, 104390.

31 S. Zhu, M. Chen, H. Dai, T. Tian, W. Pan, J. Xu and D. Lin, Safe production of rice in Cd-polluted paddy fields by rhizosphere application of zero-valent iron nanoplates at specific growth stages, *Nano Today*, 2024, **56**, 102289.

32 N. Mehrabi, A. Masud, M. Afolabi, J. Hwang, G. A. Calderon Ortiz and N. Aich, Magnetic graphene oxide-nano zero valent iron (GO-nZVI) nanohybrids synthesized using biocompatible cross-linkers for methylene blue removal, *RSC Adv.*, 2019, **9**, 963–973.

33 E. Salama, M. Samy, H. Shokry, G. El-Subruiti, A. El-Sharkawy, H. Hamad and M. Elkady, The superior performance of silica gel supported nano zero-valent iron for simultaneous removal of Cr (VI), *Sci. Rep.*, 2022, **12**, 22443.

34 Y. Z. Wang, Y. X. Deng, X. N. Liu and J. B. Chang, Adsorption behaviors and reduction strategies of heavy metals in struvite recovered from swine wastewater, *Chem. Eng. J.*, 2022, **437**, 135288.

35 X. X. Wang, L. Meng, M. Y. Hu, L. Gao and B. Lian, The competitive and selective adsorption of heavy metals by struvite in the Pb(II)-Cd(II)-Zn(II) composite system and its environmental significance, *Water Res.*, 2024, **250**, 121087.

36 Y. Z. Wang, J. R. Da, Y. X. Deng, R. Wang, X. N. Liu and J. B. Chang, Competitive adsorption of heavy metals between Ca–P and Mg–P products from wastewater during struvite crystallization, *J. Environ. Manag.*, 2023, **335**, 117552.
37 Z. P. Zhang, B. Li, F. Wicaksana, W. Yu and B. Young, Comparison of struvite and K-struvite for Pb and Cr immobilisation in contaminated soil, *J. Environ. Manag.*, 2023, **325**, 116570.
38 V. Masindi, E. Fosso-Kankeu, E. Mamakoa, T. T. I. Nkambule, B. B. Mamba, M. Naushad and S. Pandey, Emerging remediation potentiality of struvite developed from municipal wastewater for the treatment of acid mine drainage, *Environ. Res.*, 2022, **210**, 112944.
39 Y. Zhang, M. Zhao, Q. Cheng, C. Wang, H. Li, X. Han, Z. Fan, G. Su, D. Pan and Z. Li, Research progress of adsorption and removal of heavy metals by chitosan and its derivatives: a review, *Chemosphere*, 2021, **279**, 130927.
40 X. Chen, M. F. Hossain, C. Duan, J. Lu, Y. F. Tsang, M. S. Islam and Y. Zhou, Isotherm models for adsorption of heavy metals from water - a review, *Chemosphere*, 2022, **307**, 135545.
41 H. N. Tran, S. J. You, A. Hosseini-Bandegharaei and H. P. Chao, Mistakes and inconsistencies regarding adsorption of contaminants from aqueous solutions: a critical review, *Water Res.*, 2017, **120**, 88–116.
42 Y. Wei, R. Chu, Q. Zhang, M. Usman, F. U. Haider and L. Cai, Nano zero-valent iron loaded corn-straw biochar for efficient removal of hexavalent chromium: remediation performance and interfacial chemical behaviour, *RSC Adv.*, 2022, **12**, 26953–26965.
43 R. Eljamal, O. Eljamal, A. M. E. Khalil, B. B. Saha and N. Matsunaga, Improvement of the chemical synthesis efficiency of nano-scale zero-valent iron particles, *J. Environ. Chem. Eng.*, 2018, **6**, 4727–4735.
44 D. W. Cho, H. Song, F. W. Schwartz, B. Kim and B. H. Jeon, The role of magnetite nanoparticles in the reduction of nitrate in groundwater by zero-valent iron, *Chemosphere*, 2015, **125**, 41–49.
45 O. Goswami and A. A. Rouff, Interaction of divalent metals with struvite: sorption, reversibility, and implications for mineral recovery from wastes, *Environ. Technol.*, 2023, **44**, 2315–2326.
46 V. Nandre, N. Kumbhar, S. Battu, Y. Kale, A. Bagade, S. Haram and K. Kodam, Siderophore mediated mineralization of struvite: a novel greener route of sustainable phosphate management, *Water Res.*, 2021, **203**, 117511.
47 Z. Yang, N. Zhang, B. Sun, S. Su, Y. Wang, Y. Zhang, C. Wu and X. Zeng, Contradictory tendency of As(V) releasing from Fe-As complexes: influence of organic and inorganic anions, *Chemosphere*, 2022, **286**, 131469.
48 V. Manish, K. Venkata Siva, A. Arockiarajan and G. Tamadapu, Synthesis and characterization of hard magnetic soft hydrogels, *Mater. Lett.*, 2022, **320**, 132323.
49 J. Chen, R. Dong, S. Chen, D. Tang, X. Lou, C. Ye, T. Qiu and W. Yan, Selective adsorption towards heavy metal ions on the green synthesized polythiophene/MnO_2 with a synergetic effect, *J. Clean. Prod.*, 2022, **338**, 130536.
50 K. K. Hummadi, L. Zhu and S. He, Bio-adsorption of heavy metals from aqueous solution using the ZnO-modified date pits, *Sci. Rep.*, 2023, **13**, 22779.
51 Y. Yao, Y. Feng, H. Li, M. Liu, Y. Cui, C. Xu, Y. Li and J. Wang, Investigation of the adsorption performance and mechanism of multi-source mineral composite calcination materials on heavy metal ions, *Desalination*, 2024, **586**, 117847.
52 D. Wang, Y. Zhao and Q. Jia, Construction of magnetic sulfonic-functionalized hypercrosslinked polymers for efficient adsorption of azole fungicides from water, *Sep. Purif. Technol.*, 2025, **354**, 128810.
53 Z. Wang, H. Tian, J. Liu, J. Wang, Q. Lu and L. Xie, Facet-dependent adsorption of heavy metal ions on Janus clay nanosheets, *J. Hazard. Mater.*, 2024, **461**, 132548.
54 C. Wang, T. Jiang, J. Huang, M. Chen, H. Hu, L. Peng, L. Wu, Z. Chaocheng and Q. Zhang, Efficient incorporation of highly migratory thallium into struvite structure: Unraveling the stabilization mechanisms from a mineralogical perspective, *Sci. Total Environ.*, 2024, **935**, 173329.